Transitions in morphology observed in nitrogen/methane–hydrogen depositions of polycrystalline diamond films

V. M. Ayres,[a] M. Farhan, D. Spach, J. Bobbitt, J. Abdul Majeed, B. F. Wright, B. L. Wright, and J. Asmussen
Department of Electrical Engineering, Michigan State University, East Lansing, Michigan 48824

M. G. Kanatzidis
Department of Chemistry, Michigan State University, East Lansing, Michigan 48824

T. R. Bieler
Department of Materials Science and Mechanics, Michigan State University, East Lansing, Michigan 48824

(Received 2 June 2000; accepted for publication 14 February 2001)

In this work, we report on a series of transitions in morphology and texture as 5–1000 parts per million of nitrogen were added to 2% and 1% methane–hydrogen depositions of polycrystalline diamond films. Five results are reported. (1) The threshold for transition into the {100}-faceted morphology occurred at lower parts per million nitrogen for the 1% versus the 2% methane–hydrogen series, opposite from the transition thresholds previously reported. (2) At 1000 parts per million nitrogen the film quality of both series had not yet seriously degraded. (3) A well defined sequence of intermediate texture transitions as a function of increasing parts per million nitrogen was observed for both series. (4) A pretransition morphology of large crystallites interspersed among microcrystalline material directly preceding the transitions to the {100}-faceted morphology was observed for both series. (5) A layered growth and/or etched morphology at high nitrogen concentrations was observed for both series. We discuss these observations in terms of the possible influence of our deposition conditions on the accessibility of diamond growth parameter space and chemistry, including possible dynamical effects of the temperature gradients. © *2001 American Institute of Physics.* [DOI: 10.1063/1.1362406]

I. INTRODUCTION

Controlled, textured growth of polycrystalline diamond films would be desirable for many applications. Very small concentrations of nitrogen have been shown to dramatically change the morphology and crystallographic texture of polycrystalline diamond films grown using microwave plasma chemical vapor deposition (MPCVD) methods.[1–5] Previous studies have identified a sharp transition from various initial morphologies into {100}-faceted morphologies as a function of low concentrations of nitrogen. For diamond films grown in a microwave plasma tubular reactor (4 cm diam cylindrical quartz tube), an upper end concentration of nitrogen, about 400 parts per million (ppm), is reached beyond which the film crystallinity and quality are reported to degrade.[1–3,6]

In this work, a detailed study of the evolution of the morphologies and corresponding textures of methane–hydrogen grown CVD diamond films, as a function of 5–1000 ppm of nitrogen (N_2) added to the depositions, is reported. The film morphologies are investigated using TappingMode™ atomic force microscopy, and the complementary texture studies are performed using x-ray diffraction with a four-circle goniometer. Investigations are presented for two series of polycrystalline diamond films: 2% CH_4/H_2 and 1% CH_4/H_2. Five results are reported and discussed.

[a]Electronic mail: ayresv@egr.msu.edu

II. EXPERIMENTAL APPROACH

A 2.45 GHz microwave plasma cavity reactor was used to deposit polycrystalline diamond films on 7.62 cm diamond scratch-seeded (100) *p*-type silicon wafers. The Michigan State University reactor geometry is specially designed for wide-area depositions[7] up to 12.5 cm in diameter. In the present experiments, the diameter of the plasma ball was approximately 8 cm. Substrate heating is only through the formation and breaking of bonds with no external heat source. The substrate temperature depends mainly on the operating pressure, with minor dependence on the microwave input power, as discussed in Ref. 7. Therefore, the plasma volume, temperature gradients, and other parameters in our reactor system differed significantly from the tubular reactors of Refs. 1–3 as noted in Table I. The Michigan State University microwave plasma reactor system combined with a computer controlled ultrahigh vacuum and gas handling system allows careful control of the gas input variables. The nitrogen was introduced via a premixed gas of 2% N_2 in H_2. Input gases of research and ultrahigh purity, hydrogen, 99.9995%, methane, 99.99%, and hydrogen/nitrogen mix, 99.9995%, were used. Gas phase nitrogen concentrations were monitored by optical emission spectroscopy (OES) using the CN emission band. In calibration tests, an increase of 10 ppm nitrogen in the gas phase was detectable in the OES emission spectrum. The flow rates of CH_4 and H_2 were held constant at ratios of CH_4/H_2 equal to 1% and 2% while the mix of N_2/H_2 was varied. For each of these series, nitrogen

TABLE I. Comparison of reactor parameters.

Parameter	Previously reported in the literature	Present work
Area and shape	3.5 cm diam tube[a,b,c]	12.5 cm bell jar
Substrate temperature (°C)	800;[a] 830[b] Controlled by heated stage	830–860 Controlled by pressure
Reactor pressure (Torr)	37.5;[a] 165[b]	38.4
Flow rate (SCCM)	100;[a] 200[b]	204–214

[a]Reference 1.
[b]Reference 2.
[c]Reference 3.

gas was added in amounts which varied between 0 and 1000 ppm. For the zero nitrogen flow condition, we estimate an actual value of 5 ppm N_2 based on the known leak rate of laboratory air into our growth chamber of 0.25 mTorr/h. For the 1% methane–hydrogen experiments, the minimum total flow rate was 202 standard cubic centimeters per minute (sccm) for the deposition with no nitrogen introduced and the maximum total flow rate was 212 sccm for the 1000 ppm nitrogen deposition. For the 2% methane–hydrogen experiments, the minimum total flow rate was 204 sccm for the deposition with no nitrogen introduced and the maximum total flow rate was 214 sccm for the 1000 ppm nitrogen deposition.

Each sample in this study was grown for 8 h at a reactor pressure of 38.4 Torr. Our calibration experiments showed that, at our operating pressure of 38.4 Torr, the substrate temperature was approximately 825°C. The actual temperatures were also measured by a single color optical pyrometer. The samples used in this study were approximately 1 cm^2 squares cut from the center of each deposition.

A. Atomic force microscopy surface morphology measurements

TappingMode atomic force microscope (AFM) imaging and analyses were performed using a Digital Instruments™ Nanoscope IIIa operated in ambient air. Silicon tapping mode tips with nominal tip radii of 5–10 nm were used for all images. Scans 5×5 μm^2 are compared in this article; however, large-area scans, corresponding scanning electron microscopy (SEM) measurements, and optical microscopy were used to ensure that the morphologies shown in these scans are representative. The 5×5 μm^2 images were acquired using an *E*-scanner with a 13×13 μm^2 maximum scan range and the high resolution image shown in Fig. 4(b) was acquired using an *A* scanner with a 1×1 μm^2 maximum scan range.

B. Texture analysis by x-ray diffraction

The x-ray texture measurements were performed on a four-circle goniometer (Scintag XDS 2000 system) using Cu $K\alpha$ radiation at 1.54 Å with a 1 mm collimator at the x-ray source and a 2 mm slit near the detector to minimize intensity from regions away from the sample. For each sample, pole figures were measured by keeping the detector position fixed at $2\theta_{hkl}$ and rotating the sample about the axis normal to the substrate through $0°\leqslant\phi\leqslant360°$ in 5° increments (azimuth angle ϕ) and tilting the sample about an axis parallel to the substrate through $0°\leqslant\chi\leqslant80°$ in 5.0° increments (polar angle χ). Long count times of 12–25 s/datum were used to minimize the noise due to background from the substrate. The four-circle goniometer was used to measure (111), (220), and (400) pole figures. The pole figures were corrected using an analytical defocusing curve which approximates the more complex actual defocusing optics. Therefore the measured textures are suitable for comparison, but they also contain small systematic errors particularly at high tilt angles. Data reduction to obtain the orientation distribution functions was done assuming only mirror symmetry using standard procedures with popLA software.[8] Inverse pole figures were extracted from the projection of the sample orientation distribution.[8]

III. RESULTS

A. 2% methane–hydrogen series

The major transitions in morphology for the 2% methane–hydrogen series as a function of increasing ppm N_2 are shown in Fig. 1. The 2% methane–hydrogen depositions showed a uniform coverage of microcrystalline material between about 5 and 150 ppm nitrogen. Large crystallites interspersed among the microcrystalline material appeared with about 175–225 ppm nitrogen. The surface morphology changed abruptly into a {100}-faceted morphology between 225 and 250 ppm nitrogen. The 2% series remained in {100}-faceted morphologies after the initial transition. With 900–1000 ppm N_2, rounded and scalloped edges of the {100}-faceted crystallites and a layered morphology were observed. Raman spectroscopy of the 2% series, reported elsewhere,[9] showed unambiguous diamond peaks with full widths half maxima (FWHMs) of 6–10 cm^{-1} for all films after the initial transition into well-faceted material, including those with 900–1000 ppm N_2 in the depositions. Broad peaks were observed for the pretransition microcrystalline material. A minimum value of 6.3 cm^{-1} was observed at 400 ppm nitrogen. All other posttransition FWHM values were about 10 cm^{-1}. No progressive deterioration of the film quality was observed as a function of increasing ppm nitrogen.

The influence of the increasing ppm N_2 on texture development after the transition into well-faceted morphologies is shown in Fig. 2 for the 2% methane–hydrogen series. Texture is defined here as the distribution of crystallographic vectors aligned with the normal direction. The samples grown with 5 ppm nitrogen had a strong ⟨101⟩ texture component and a weaker ⟨203⟩ texture component. With increasing nitrogen up to 225 ppm, the ⟨203⟩ component strengthened and the ⟨101⟩ component weakened. With 250 ppm nitrogen, a broad ⟨102⟩ peak developed and the ⟨203⟩ and ⟨101⟩ components weakened (we note that the abrupt morphology transition to square facets occurred with 250 ppm nitrogen). With increasing nitrogen up to 400 ppm, a band of orientations between ⟨102⟩ and ⟨114⟩ developed. With 500 ppm nitrogen, strong ⟨001⟩ and ⟨104⟩ components developed, with retention of the strong ⟨114⟩ component and loss of the

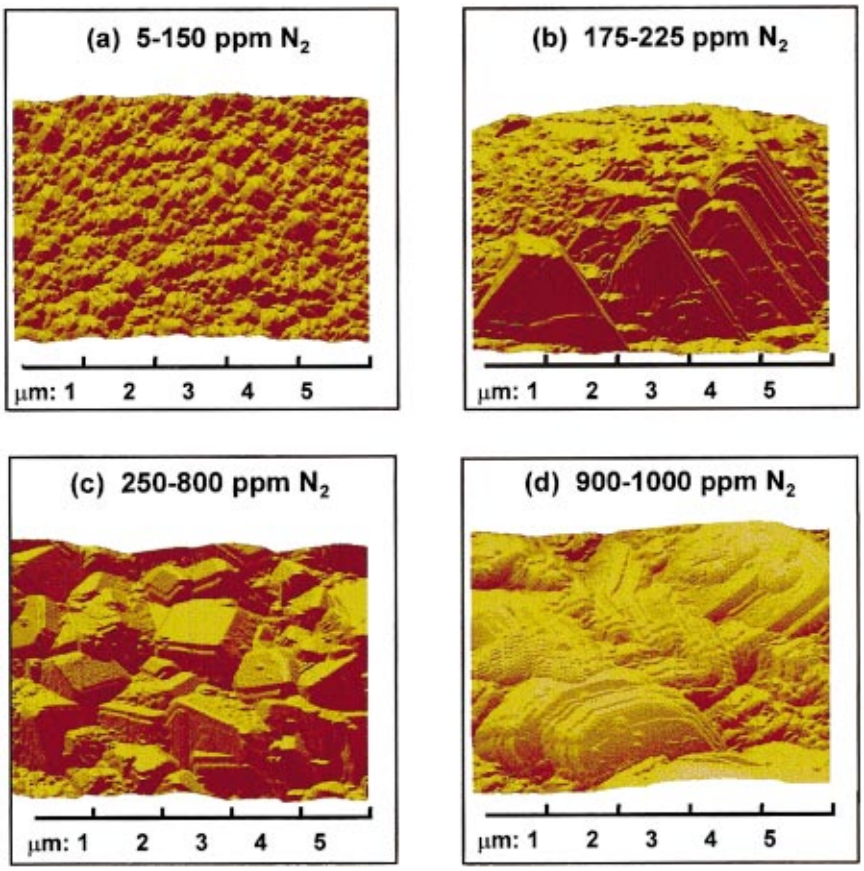

FIG. 1. (Color) Major transitions in morphology of the 2% methane–hydrogen series as a function of increasing ppm N_2 showing (a) microcrystalline morphologies; (b) microcrystalline morphologies and micron-sized individual crystallites; (c) (100)-faceted morphologies; (d) etched/layered growth of large (100)-faceted crystallites. The zero nitrogen flow condition is estimated as 5 ppm N_2 based on the known leak rate of the reactor.

⟨102⟩ component. With increasing nitrogen from 600 through 1000, a band of orientations between ⟨104⟩ and ⟨114⟩ was consistently observed, but the additional strong ⟨001⟩ component was only observed for the samples grown with 500 and 700 ppm nitrogen. We note that the minimum FWHM of the Ref. 9 Raman measurements corresponded more closely with the first transition to ⟨001⟩ texture between 400 and 500 ppm N_2 than with the observed transition in morphology at 250 ppm N_2.

B. 1% methane–hydrogen series

The major transitions in morphology for the 1% methane–hydrogen series as a function of increasing ppm N_2 are shown in Fig. 3. The 1% methane–hydrogen depositions showed a uniform coverage of well-faceted, small (less than 0.5 μm^2) crystallites with 5 ppm nitrogen. The small crystallites appeared to be mainly of the roof-shaped morphology that has a ⟨101⟩ direction close to the sample normal, an observation which was supported by the x-ray texture analysis. (For a [101] direction, there are two ⟨111⟩ directions with 35.3° inclination: [111] and $[\bar{1}11]$. The corresponding faces form roof-shaped structures that can be observed in AFM or SEM images of the surfaces of these diamond films.) With 25 ppm, the morphology changed into one of larger crystallites interspersed among a smaller crystallite field. With 50 ppm nitrogen, a transition into a uniform coverage of larger micron-sized crystallites was observed. These appeared to be mainly roof-shaped morphologies. With 75 ppm nitrogen, micron-sized crystallites with roof-shaped morphologies were still observed but a few micron-sized {100}-faceted crystallites were interspersed among them. A uniform coverage of micron-sized {100}-faceted crystallites occurred with 100 ppm nitrogen.

The crystallite morphologies of the depositions with 100–1000 ppm nitrogen all showed {100}-faceted surface morphologies. However, for the depositions with 300, 400, and 500 ppm nitrogen, the surface morphology varied from place to place over a millimeter-sized area similar to the x-ray measurement area. For example, in the lower part of Fig. 3(e), multiple facets are observed with the same orientation for both roof-top and square faceted morphologies. From 600 to 1000 ppm nitrogen, the morphologies again had the appearance of a uniform coverage of well-faceted crystallites with {100} facets on the surface. For the 700–1000 ppm nitrogen depositions, rounded and scalloped edges were observed on the {100} facets, with a layered appearance on the (100) surfaces. The rounded and scalloped edges and the layering were observed at lower ppm N_2 and were more pronounced in the 1% series than in the 2% series. This was also observed in a SEM analysis of the same samples previously reported in Ref. 9. Details of this morphology are shown in the AFM images of Fig. 4. Raman spectroscopy of the 1% series, reported in Ref. 9, showed unambiguous diamond peaks with FWHMs of 6–15 cm^{-1} for all of the films (none were microcrystalline). A minimum value of 6.1 cm^{-1} was observed at 200 ppm nitrogen. All other posttransition FWHM values were about 12 cm^{-1}. No progressive deterio-

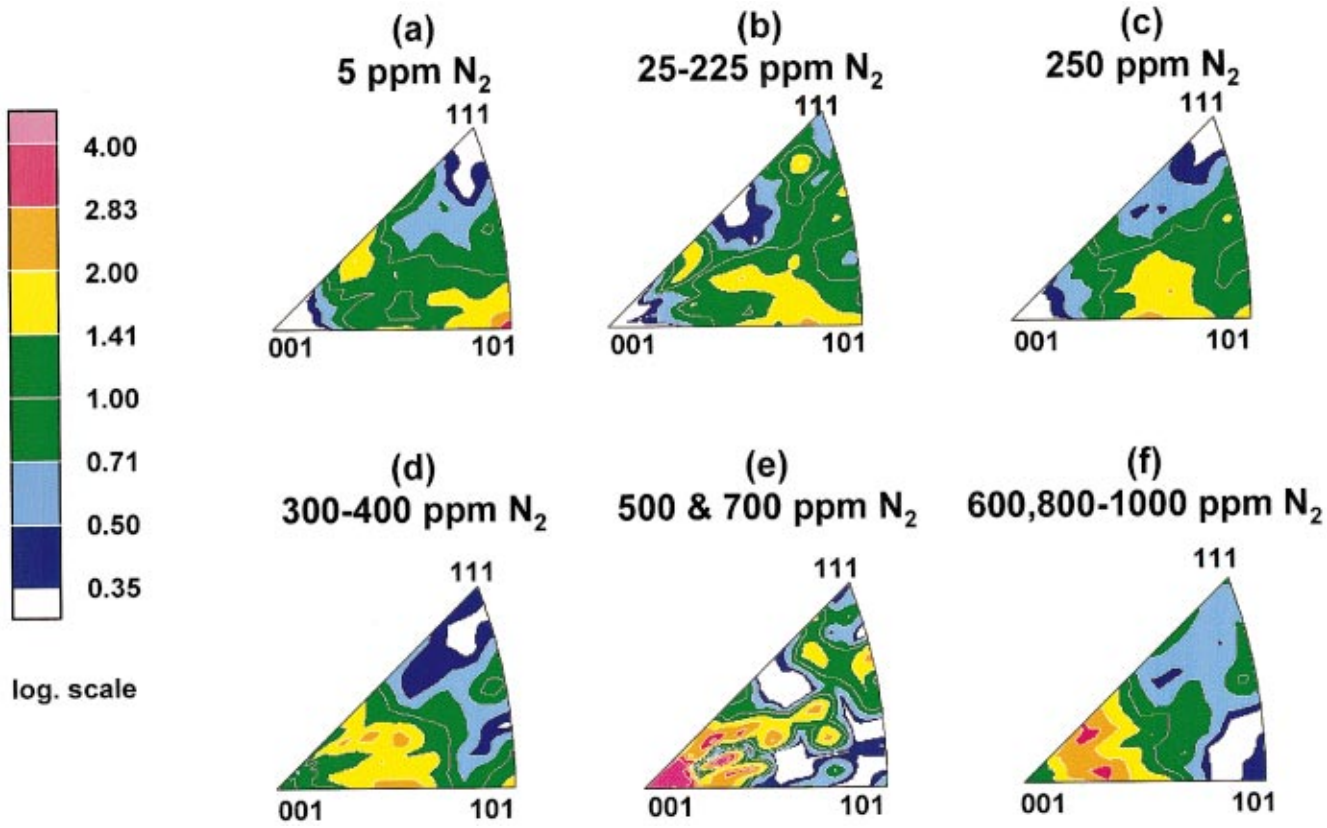

FIG. 2. (Color) Texture development of the 2% methane–hydrogen series as a function of increasing ppm N_2. Equal area projections are used. All inverse pole figures are shown at 4× random. (a) Initial ⟨101⟩ texture. (b) Strengthening ⟨203⟩ texture component. (c) Strengthening ⟨102⟩ texture component at the transition into (100)-faceted morphology. (d) First development of a ⟨104⟩–⟨114⟩ band of orientations. (e) Development of a ⟨001⟩ texture component, with ⟨102⟩ and ⟨114⟩ components also evident. (f) ⟨104⟩–⟨114⟩ texture band.

ration of the film quality was observed as a function of increasing ppm nitrogen.

The influence of the increasing N_2 on texture development is shown in Fig. 5 for the 1% methane–hydrogen series. The observed changes in texture mirrored the changes observed for the 2% methane–hydrogen series but the transitions occurred at systematically lower levels of nitrogen. Once again, the minimum FWHM of the Ref. 9 Raman measurements corresponded more closely with the first transition to ⟨001⟩ texture with 200 ppm N_2 than with the observed transition in morphology at 100 ppm N_2.

One difference for the 1% methane–hydrogen series was that a multicomponent texture was observed for the samples grown with 300–500 ppm nitrogen which correlated with the multiple types of facet morphologies observed on these samples. Another difference was that the high nitrogen ⟨114⟩–⟨104⟩ band was stronger for the 1% methane–hydrogen series and that an additional strong ⟨001⟩ texture component was observed three times, at 200, 800, and 1000 ppm nitrogen.

IV. DISCUSSION OF RESULTS

We report the following five results.

(1) The threshold for transition into the {100}-faceted morphology occurred at lower ppm N_2 for the 1% than for the 2% methane–hydrogen series, opposite from that which has been reported in a tubular reactor.[1–3]

Table I shows the differences in reactor conditions between our reactor and those of Refs. 1–3. Important variables affecting the formation, concentrations, and resonance times of the various chemical species present may have been very different, despite similarities in the methane–hydrogen ratios and substrate temperatures. Therefore, we cannot interpret the effect of nitrogen in our reactor in terms of its influence on the previously reported (100)/(111) competitive growth parameter curves.[10–13] In this previously reported work, a transition into crystallites with small (100)-faceted surfaces and $<5°$ tilt was observed, from which a corresponding transition in growth rate parameter $\alpha = \sqrt{3}\, v_{100}/v_{111}$ from about 1.5 to near 3.0 was postulated. In our work, we observe crystallites with large (100)-faceted surfaces and often a band of orientations between ⟨104⟩ and ⟨114⟩. This band structure corresponds to (100) faces with a tilt of 14.04° towards ⟨010⟩ and a tilt of 19.47° towards ⟨111⟩. We are exploring the possibility that the corresponding transition in growth parameter α may be in the opposite sense, from about 1.7 to 1.5.

(2) At 1000 parts per million nitrogen the film quality of both series had not seriously degraded, which is the highest value reported to date.

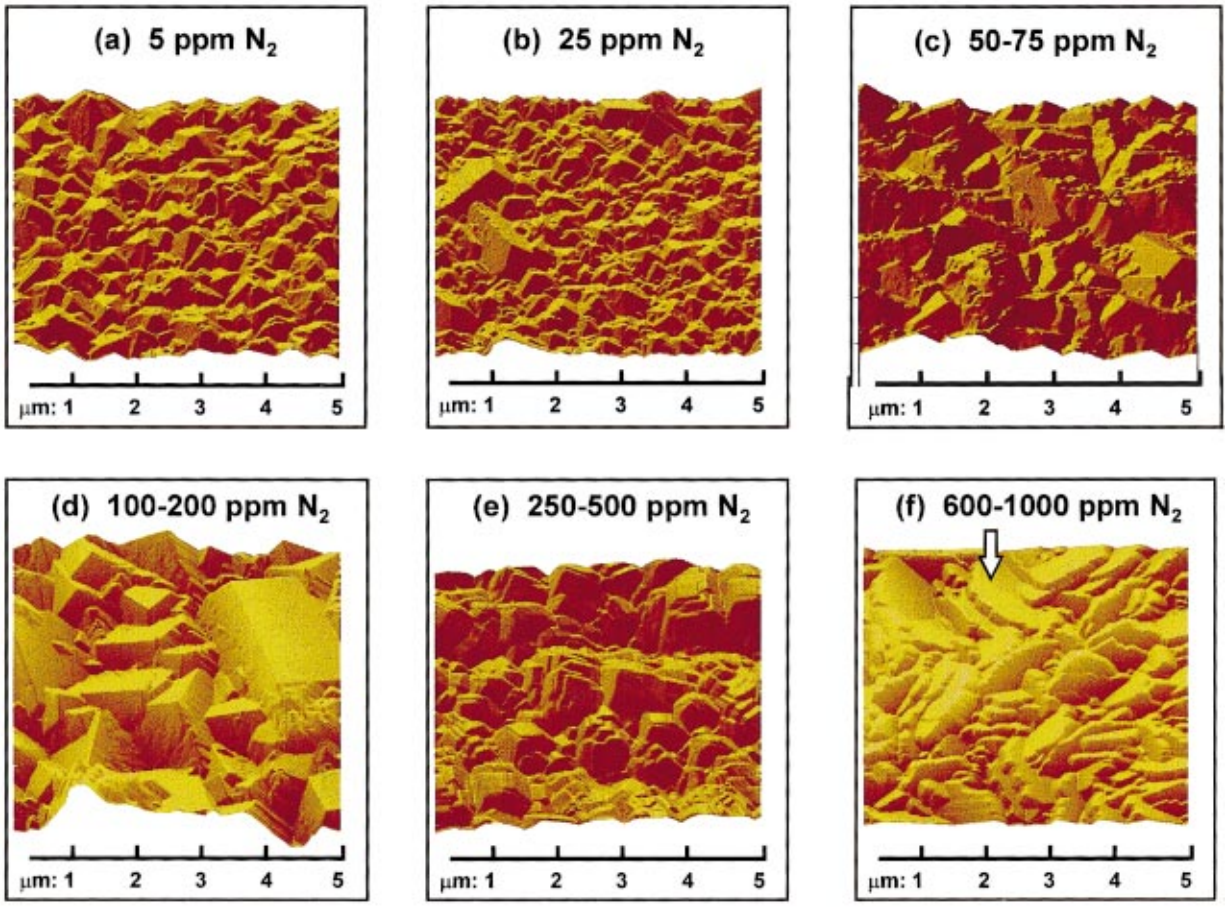

FIG. 3. (Color) Major transitions in morphology of the 1% methane–hydrogen series as a function of increasing ppm N_2 showing (a) submicron roof-shaped morphologies; (b) submicron crystallites and micron-sized individual crystallites; (c) micron-sized, roof-shaped morphologies; (d) micron-sized (100)-faceted morphologies; (d) multicomponent growth; (e) etched/layered growth of large (100)-faceted crystallites.

The difference in reactor geometry from narrow to wide area may be responsible for the high gas phase nitrogen tolerance without loss of diamond film quality by decreasing the concentration of nitrogen over a given surface area. This has allowed us to see the sequence of transitions and texture in more detail than has been previously reported.

(3) A well defined sequence of intermediate texture transitions was observed for the evolution from an initial

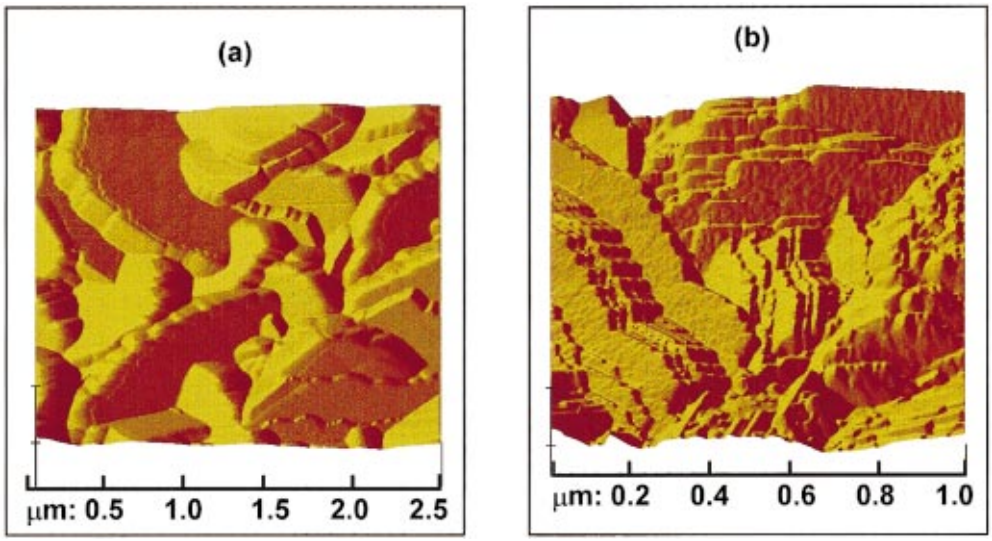

FIG. 4. (Color) Details of the etched/layered morphology observed at high ppm N_2. The images shown are from the 1% methane–hydrogen, 1000 ppm N_2 sample. (a) 2.5×2.5 μm^2 *E*-scanner AFM image of a crystallite edge, corresponding to the arrow-marked region of Fig. 3(f); (b) 1.0×1.0 μm^2 *A*-scanner AFM image of the same sample showing the layers and edges.

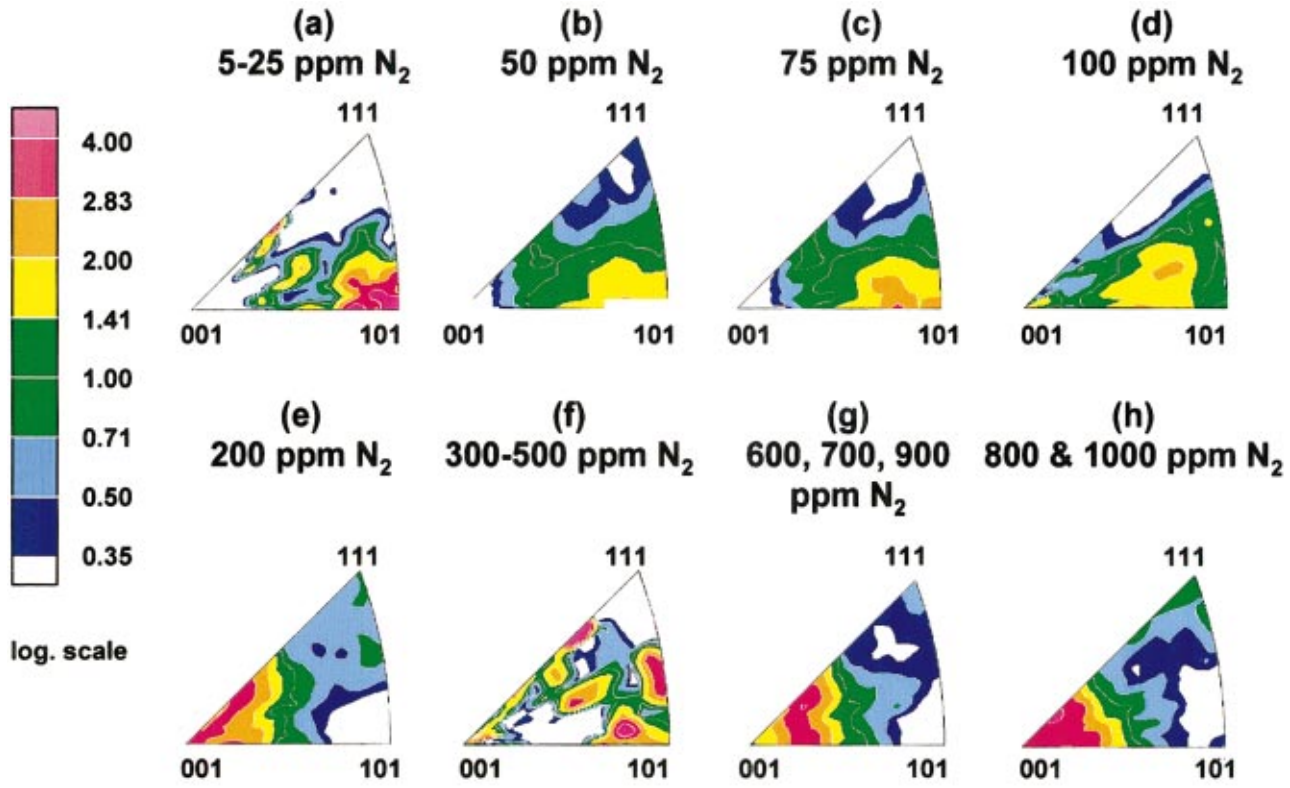

FIG. 5. (Color) Texture development of the 1% methane–hydrogen series as a function of increasing ppm N_2. Equal area projections are used. All inverse pole figures are shown at 4× random. (a) Initial ⟨101⟩ texture. (b) Initial development of a ⟨203⟩ texture component. (c) Strengthening ⟨203⟩ texture component. (d) Strengthening ⟨102⟩ component at the transition into (100)-faceted morphology. (e) Initial development of a ⟨104⟩–⟨001⟩–⟨114⟩ texture range. (f) Multicomponent texture. (g) ⟨104⟩–⟨114⟩ band of orientations. (h) ⟨104⟩–⟨001⟩–⟨114⟩ texture range.

⟨101⟩ texture to a final range of orientations between ⟨104⟩–⟨001⟩–⟨114⟩ for both the 2% and 1% methane–hydrogen series as a function of increasing parts per million nitrogen.

The sequence of crystal orientation transitions indicates a shift from ⟨101⟩ to near-⟨001⟩ texture, as has been reported in prior work.[1–6,9] We have observed and reported that specific crystal orientations *between* ⟨101⟩ and ⟨001⟩ are sequentially stabilized with increasing nitrogen. This implies that either (111) or (001) crystal planes have preferred growth advantages that may depend on different reactions that are favored with a particular concentration of nitrogen. With sufficient nitrogen, orientations near ⟨001⟩ but commonly closer to ⟨104⟩ and ⟨114⟩ have the highest growth advantage, such that these crystal orientations dominate. However, under some conditions many orientations may be stabilized, such as in Figs. 2(e) and 5(f), suggesting that different reactions occurred preferentially on different orientations. Similar phenomena have been observed in related studies with different growth times.[14] Finally, similar transitions for the 1% methane series occur at about half of the nitrogen concentration for the 2% methane conditions. These observations all suggest that particular concentrations of nitrogen are needed to promote growth of a favored crystal orientation by means of a distinct stoichiometric reaction path. We are currently investigating molecular models of how nitrogen could change the specific reaction paths for ⟨110⟩ nucleation and growth which are described in Ref. 15.

(4) A pretransition morphology of large crystallites interspersed among microcrystalline material which seemed to directly precede the transitions to the {100}-faceted morphology was observed for both the 2% and 1% methane–hydrogen depositions.

(5) A layered growth and/or etching at high nitrogen concentrations was observed for both the 2% and the 1% methane–hydrogen depositions.

We are investigating the possibility that nitrogen, acting as a mineralizer or chemical vapor transport agent, may account for these observations. A mineralizing agent ''*X*,'' added to the main deposition, promotes both the dissolution of a solid and its redeposition via a reversible reaction,

$$A_{\text{solid}} + X_{\text{gas}} \underset{k_2,T_2}{\overset{k_1,T_1}{\rightleftarrows}} (AX)_{\text{gas}}, \tag{1}$$

where T_i is the temperature and k_i is the rate constant. Such processes are known to occur in gas phase systems and to promote the growth of well formed large crystals in a large variety of materials.[16–21] In the gas phase case, a chemical vapor transport reaction is enabled by the added mineralizer. Being reversible, depending on the temperature, these reactions can quickly convert large quantities of microcrystalline material into large crystallites. Previous studies of a similar 2.45 GHz diamond deposition reactor[22] have shown a radial temperature gradient from center to edge of about 100 °C/

cm, and a vertical temperature gradient across the plasma sheath of about 600 °C/cm. While the nitrogen plasma chemistry might have altered these numbers, we would still expect similar gradients to have been present during growth of the samples in the present work. Additional temperature fluctuations, associated with the cyclic nature of diamond film growth,[23] could also be present.

The possibility of using chemical vapor transport for diamond growth has been investigated theoretically[24] and experimentally[25] using a two zone furnace (for T_1 and T_2) and a graphite carbon source. The dissolution of graphite in molecular hydrogen, nitrogen, oxygen, or chlorine gases was calculated theoretically from thermodynamic principles. Hydrogen showed the greatest promise of acting as a chemical vapor transport agent, and was experimentally investigated. These experiments demonstrated the conversion of the graphite into diamond by the mechanism shown in Eq. (1). Because the calculations indicated that the graphite would not dissolve readily in N_2, this case was not experimentally investigated. Neither calculations nor experiments were performed for the case where microcrystalline $\langle 101 \rangle$ textured diamond is the carbon source. Therefore, these studies, which are the closest we can find to our own, are not directly comparable but they do indicate that chemical vapor transport reactions can play a role in diamond deposition when temperature gradients are present.

The hypothesis that N or a $N-H_x$ species acts as a mineralizer in a gas phase chemical vapor transport reaction would account for several of our observations. A mineralizer would react preferentially with highly energetic sites such as points and edges, and defective material. This effect is consistent with the observed pretransition morphology, large crystallites interspersed in a field of finer-grained material, which seemed to precede the transitions to the {100}-faceted morphology for both the 2% and 1% methane–hydrogen grown films. A similar pretransition morphology has recently been reported by another group.[6] There would be a threshold concentration of mineralizer associated with the onset of the growth of larger well-formed crystals. Above the threshold, an optimum concentration, or range of concentrations, would be present. Beyond this range, growth could become unstable if dissolution were comparable. This could account for both the ledges and the unusually large crystallite sizes observed at high ppm nitrogen for both the 2% and the 1% methane–hydrogen depositions. The reversibility of a mineralizer reaction would also account for the observation that only parts per million of nitrogen are needed to induce the large changes in morphology reported by ourselves and by others, since the mineralizing agent would become free to participate again (acting catalytically) in the dissolution of defective material and small crystallites at temperature T_1.

V. SUMMARY

Detailed observations of a series of transitions in morphology and crystallographic texture as ppm N_2 were added to 2% and 1% methane–hydrogen depositions of diamond films have been reported in this article. These results suggest that the concentration of nitrogen promotes growth of particular crystal orientations over others, leading to a growth advantage for well defined low-index crystal orientations. We are investigating the hypothesis that plasma-generated $N-H_x$ species act as mineralizing/chemical vapor transport agents that deposit, remove, and redeposit carbon on the film surface.

[1] R. Locher, C. Wild, N. Herres, D. Behr, and P. Koidl, Appl. Phys. Lett. **65**, 34 (1994).
[2] W. Muller-Sebert, E. Worner, F. Fuchs, C. Wild, and P. Koidl, Appl. Phys. Lett. **68**, 759 (1996).
[3] C. Wild, R. Locher, and P. Koidl, Mater. Res. Soc. Symp. Proc. **416**, 75 (1996).
[4] S. Jin and T. D. Moustakas, Appl. Phys. Lett. **65**, 403 (1994).
[5] S. Bohr, R. Haubner, and B. Lux, Appl. Phys. Lett. **68**, 1075 (1996).
[6] A. Floter, H. Guttler, C. Lutz-Elsner, A. Bergmaier, and C. Dollinger, Diamond99, Prague, Czech Republic, 12–17 September 1999, Abstract Book 3.1.
[7] S. Khatami, Ph.D. thesis, Michigan State University, East Lansing, MI, 1997.
[8] J. S. Kallend, U. F. Kocks, A. D. Rollett, and H.-R. Wenk, Mater. Sci. Eng., A **132**, 1 (1991).
[9] J. Asmussen, J. Mossbrucker, S. Khatami, W. S. Huang, B. Wright, and V. Ayres, Diamond Relat. Mater. **8**, 220 (1999).
[10] C. Wild, R. Kohl, N. Herres, W. Muller-Sebert, and P. Koidl, Diamond Relat. Mater. **3**, 373 (1994).
[11] C. Wild, P. Koidl, W. Muller-Sebert, H. Walcher, R. Kohl, N Herres, R. Locher, R. Samlenski, and R. Brenn, Diamond Relat. Mater. **2**, 168 (1993).
[12] C. Wild, P. Koidl, N. Herres, W. Muller-Sebert, and T. Eckermann, *Proceedings of the 2nd International Symposium on Diamond Materials*, edited by A. J. Purdes, J. C. Angus, R. F. Davis, B. M. Meyerson, K. E. Spear, and M. Yoder (The Electrochemical Society, Pennington, NJ, 1991), Vol. 91–8, p. 224.
[13] C. Wild, N. Herres, and P. Koidl, J. Appl. Phys. **68**, 973 (1990).
[14] V. M. Ayres *et al.*, Diamond Relat. Mater. **9**, 236 (2000).
[15] C. C. Battaile, D. J. Srolovitz, and J. E. Butler, Diamond Relat. Mater. **6**, 1198 (1997).
[16] M. Lenz and R. Gruehn, Chem. Rev. **97**, 2967 (1997).
[17] R. Neddermann and M. Binnewies, Z. Anorg. Allg. Chem. **622**, 17 (1996); R. Neddermann, S. Gerighausen, and M. Binnewies, *ibid.* **622**, 21 (1996).
[18] M. Weil and R. Glaum, Eur. J. Solid State Inorg. Chem. **35**, 495 (1998); R. Glaum, Z. Kristallogr. **205**, 69 (1993).
[19] Y. K. Rao, High Temp. Mater. Sci. **34**, 293 (1995).
[20] M. Lencka and R. Riman, Chem. Mater. **5**, 61 (1993).
[21] R. Laudise, Chem. Eng. News **65**, 30 (1987).
[22] K. Hassouni, T. A. Grotjohn, and A. Gicquel, J. Appl. Phys. **86**, 134 (1999); W. Tan and T. Grotjohn, Diamond Relat. Mater. **4**, 1145 (1995).
[23] K. Kobashi, K. Nishimura, Y. Kawate, and T. Horiuchi, Phys. Rev. B **38**, 4067 (1988).
[24] W. Piekarczyk, R. Roy, and R. Messier, J. Cryst. Growth **98**, 765 (1989).
[25] W. Piekarczyk, R. Messier, R. Roy, and C. Engdahl, J. Cryst. Growth **106**, 279 (1990).